Magnetic and magneto-optic properties of lead- and bismuth-substituted yttrium iron garnet films

P. Hansen, K. Witter, and W. Tolksdorf

Philips GmbH Forschungslaboratorium Hamburg, D-2000 Hamburg 54, Federal Republic of Germany

(Received 27 December 1982)

The saturation magnetization M_s, the uniaxial anisotropy K_u, the optical absorption α, the Faraday rotation θ_F, and the Faraday ellipticity ψ_F of epitaxial garnet films of composition $Y_{3-x}Bi_xFe_5O_{12}$ and $Y_{3-y}Pb_yFe_5O_{12}$ have been investigated for $x \leq 1.7$ and $y \leq 0.25$. The magnetostriction constants $\lambda_{100}, \lambda_{111}$ and the cubic anisotropy K_1 were studied on flux-grown crystals for $x \leq 1$. The temperature dependence of M_s, K_1, K_u, λ_{100}, λ_{111}, and θ_F, ψ_F at 633 nm has been measured in the range $4.2 \text{ K} \leq T \leq T_c$. The concentration dependence of these properties is linear. In particular, the contribution of the bismuth and lead to the Faraday rotation $\Delta\theta_F/x$ and $\Delta\theta_F/y$ at $\lambda = 633$ nm turned out to be $-25\,400$ and $-18\,500$ deg cm^{-1} at $T = 4.2$ K and $-20\,600$ and $-18\,400$ deg cm^{-1} at $T = 295$ K, respectively. The temperature dependence of θ_F and ψ_F can be described in terms of the sublattice magnetizations inferred from the fit of the molecular-field theory to the measured saturation magnetization. The extracted magneto-optical coefficients reveal a nonlinear concentration dependence. The magnitude of the growth-induced anisotropy is essentially controlled by the supercooling of the melt for both the lead- and bismuth-substituted films. The temperature dependence of K_u^g is discussed in terms of the single-ion theory.

I. INTRODUCTION

The development of new device applications based on high magneto-optical effects of bismuth-substituted iron garnets have intensified the study of the basic properties of these materials. In particular, garnet compositions suitable for displays,[1-4] printers,[5] bubble applications,[6-9] gyrolasers,[10] or optical-communication components[11] have received special attention. Thereby different properties which are affected by lead and bismuth are of importance for such applications and thus their understanding and control is of significant interest. In particular, the Curie temperature, the growth-induced anisotropy, the magnetostriction constants, the optical absorption, and the Faraday rotation and ellipticity are known to be strongly affected by the lead and bismuth content. For yttrium iron garnet substituted with these ions primarily the wavelength dependence of the magneto-optical properties has been investigated[12] where essentially polycrystalline[13-17] and flux-grown crystals[18,19] were considered. The temperature dependence of the magneto-optical properties and the growth-induced anisotropy, however, have not yet been studied for these compositions although they are of significant relevance for technical applications. Recent progress in the growth of substituted gadolinium,

samarium, and neodymium gallium garnet substrates with high lattice constants[20] now permits the growth of epitaxial bismuth-substituted yttrium iron garnet films of almost any Bi content up to the solubility limit. The availability of these garnets and the interest in the temperature behavior have led to the results presented in this paper concerning the effects induced by the lead and bismuth in correspondence to the investigations reported for the lead- and bismuth-substituted gadolinium iron garnet system.[21-24]

The experimental results are presented in Sec. II. In Sec. III these results are discussed and interpreted in terms of the molecular field theory and the single-ion theory.

II. EXPERIMENTAL RESULTS

A. Garnet material characterization

The garnet films of composition

$$Y_{3-y}Pb_yFe_{5-z}Pt_zO_{12}$$

and

$$Y_{3-x-y}Bi_xPb_yFe_{5-z}Pt_zO_{12}$$
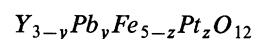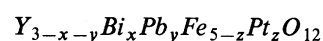
were grown by liquid-phase epitaxy (LPE) onto (111) oriented Ca-, Mg-, Zr-substituted gadolinium, samarium, or neodymium gallium garnet substrates

TABLE I. Cation ratios of the melts used to grow the investigated lead- and bismuth-substituted iron garnet films.

Cation ratios	Melt composition				
	A	B	C	D	E
Y:(Bi + Pb + B + Fe)	0.0109	0.0069	0.0075	0.0096	0.0053
(Bi + Pb):B	7.12	8.52	6.01	6.78	12.00
Pb:Bi		5.78	1.54	1.16	1.54

with lattice constants ranging between 1.2380 nm $\leq a_s \leq$ 1.2508 nm.[20,25] To provide a small room-temperature misfit the substrates were selected according to the expected lattice constant of the film. These were grown from a supersaturated melt using the horizontal dipping mode and a rotation rate of 90 rotations per min. The direction of rotation was reversed every four sec.[26] Since the incorporation of substituents like bismuth and lead strongly depends on the melt composition[27] the starting melt composition for yttrium iron garnet based on PbO-B_2O_3 (Ref. 26) was changed by Bi_2O_3 additions and by a stepwise alteration of the cation ratios. The investigated films were grown from five melts with cation ratios given in Table I. Further melts A^* were used containing an increased iron excess with respect to melt A. The solubility product $L_s = [Y]^3 \times [Fe]^5$ of A^* was kept constant and the ratio [Fe]/[Y] varied between 12 (melt A) and 40 (Ref.

27). The growth temperatures ranged between 950 and 1200 K. The film composition was controlled by the choice of the melt and the variation of the supercooling and was determined by electron probe microanalysis (EPMA).[28] The measured analysis data of selected film compositions used for the temperature-dependent measurements are compiled in Table II together with the supercoolings ΔT_s. The given errors apply for middle and high substitutional levels and are much lower for low x, y, and z values. The data reveal a linear variation of bismuth content with ΔT_s for each melt composition while the platinum content also increases linearly with ΔT_s but approximately independent of the melt composition. The lead behaves differently showing a strong nonlinear increase of the content versus ΔT_s.

The lattice constants a of the films given in Table II were calculated from the misfit $\Delta a^\perp$ and the sub-

TABLE II. Supercooling ΔT_s, chemical analysis data, lattice constant a and thickness L of epitaxial garnet films of composition $Y_{3-y}Pb_yFe_{5-z}Pt_zO_{12}$ and $Y_{3-x-y}Bi_xPb_yFe_{5-z}Pt_zO_{12}$. (a) Grown from melt A; (b) grown from melt B; (c) grown from melt C; (d) grown from melt D; (e) estimated; (f) error: ±0.005 because of $\Delta a^\perp \approx 0$.

Sample no.	ΔT_s (K)	x	y	z	a (nm)	L (μm)
1[a]	3	0	0.006	0.005	1.2378	6.8
2[a]	20	0	0.013	0.011	1.2378[f]	10.7
3[a]	50	0	0.051	0.016	1.2383[f]	6.7
4[a]	70	0	0.084	0.019	1.2387	8.2
5[a]	101	0	0.143	0.026	1.2394[f]	10.3
6[a]	141	0	0.246	0.032	1.2404	5.3
7[b]	5	0.06	0.011	0.007	1.2383[f]	4.6
8[b]	10	0.10	0.020	0.012	1.2388	6.1
9[b]	59	0.24	0.044	0.014	1.2401	5.0
10[b]	100	0.41	0.092	0.021	1.2418	4.6
11[b]	153	0.65	0.189	0.024	1.2427	4.3
12[c]	43	0.73	0.034	0.025	1.2439	4.3
13[c]	73	1.03	0.047	0.023	1.2461	2.7
14[c]	95	1.25	0.063	0.032	1.2489	3.0
15[c]	113	1.44	0.080	0.030	1.2504[f]	2.3
16[c]	135	1.54	0.098	0.024	1.2509[f]	2.2
17[d]	150[e]	1.71	0.130	0.036	1.2514[f]	2.7
Error	±2	±0.03	±0.01	±0.005	±0.0001	±5%
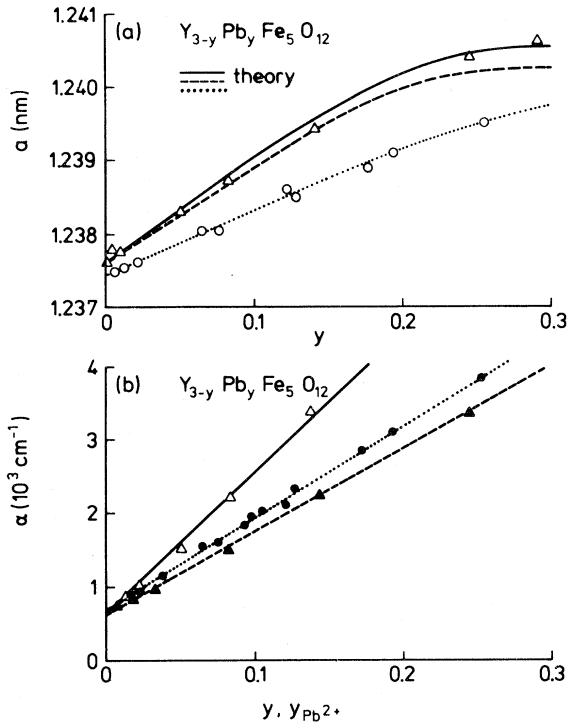
FIG. 1. Dependence of (a) the lattice constant and (b) the optical absorption at $\lambda = 633$ nm on the lead content for films grown from melt A. The solid, dashed, and dotted line in (a) were calculated from the ionic radii[30] for the case that the Pb^{2+} and Pb^{4+} ions only occupy dodecahedral sites (dashed line), a part of the Pb^{4+} ions enter octahedral sites (solid line), and that a fraction of Fe^{3+} ions occupy dodecahedral sites (dotted line). The dashed and dotted line in (b) represents α vs y and the solid line α vs $y_{Pb^{2+}}$. The circles in (a) and (b) represent data of films grown from melt $A^*([Fe]/[Y] > 12)$ indicating that a fraction of Fe^{3+} ions enter dodecahedral sites.

strate lattice constant a_s (Refs. 22 and 29) using the relation $a = a_s - [(1-\mu_{111})/(1+\mu_{111})]\Delta a^\perp$ where μ_{111} is the Poisson constant for (111)-oriented films and $(1-\mu_{111})/(1+\mu_{111}) = 0.538$ which applies for pure $Y_3Fe_5O_{12}$. The results for lead substitutions are shown in Fig. 1(a). The nonlinearity has to be attributed to the increasing Pb^{4+} concentration maintaining charge compensation as with increasing lead content the Pt^{4+} content turns out to remain nearly constant. The measured lattice constants are in good agreement with those calculated from the ionic radii[30] (dashed and solid line). The dashed line was calculated assuming the Pb^{2+} and the Pb^{4+} ions to enter only dodecahedral sites. The solid line was obtained assuming an increasing fraction of Pb^{4+} ions to occupy octahedral sites which for $y = 0.3$ is about 20% of the total Pb^{4+} content. In both cases

the platinum content was taken from an interpolating curve through the experimental data given in Table I. The ionic radii for Y^{3+}, Pb^{2+}, and Pb^{4+} were taken from Ref. 31 yielding for pure $Y_3Fe_5O_{12}$ a lattice constant of 1.237 63 nm which is in good agreement with the experimental value of our films. This fractional occupation of octahedral sites by Pb^{4+} ions was already found for lead-substituted gadolinium iron garnets.[21,23] These films exhibit no detectable fraction of Y^{3+} ions on octahedral sites. From electron microprobe analysis there is a vague evidence, that an increasing part of iron (in the order of some per mille) is entering dodecahedral sites when the ratio [Fe]/[Y] is increased.[27] This is confirmed for films which were grown from a melt with [Fe]/[Y] = 20 (Ref. 32).

The circles represent films grown from melt A^* ([Fe]/[Y] > 12). The considerably lower data of a indicate a small fraction of Fe^{3+} ions to occupy dodecahedral sites. A comparison with calculated radii (dotted line) yields about 0.01 Fe^{3+} ions per formula unit on c sites. The charge compensation by Pb^{4+} ions in addition can be concluded from the optical absorption and magneto-optical measurements since essentially the Pb^{2+} ions contribute to these effects.[23,24] The optical absorption is displayed in Fig. 1(b) where α is plotted versus Pb^{2+} content $y_{Pb^{2+}} = \frac{1}{2}(y + z)$ and versus total lead content y at $\lambda = 633$ nm. For both cases a linear relationship is obtained. These results together with the dependence of the Faraday rotation and Faraday ellipticity on the lead content suggests that the presence of other charge compensating ions such as Fe^{4+} instead of Pb^{4+} appears to be unlikely. It should be mentioned, however, that for $Gd_{3-y}Pb_yFe_5O_{12}$ films this linear dependence of α on the Pb^{2+} content occurs at shorter wavelengths.[24] From extrapolation of α to $y = 0$ for the films grown from melt A the optical absorption for the lead-free $Y_3Fe_5O_{12}$ is obtained yielding $\alpha = 620$ cm^{-1} for $T = 295$ K and $\lambda = 633$ nm.

The lattice constants for the bismuth-substituted films are shown in Fig. 2. The solid symbols represent literature data[13,18,33–37] primarily from polycrystalline garnets. These values appear to be slightly lower at high x values as compared to the film data. This is caused by the lead content of the films. The calculated lattice constants (solid line) were obtained with a radius of the bismuth ion of $r = 0.117$ nm. The highest bismuth content which was attained in these films was $x = 1.71$. A further increase of the bismuth content beyond the highest value reported for polycrystalline materials of $x = 1.88$ (Ref. 38) requires different growth conditions and substrates with a higher lattice constant. However, if the attainable maximum bismuth con-
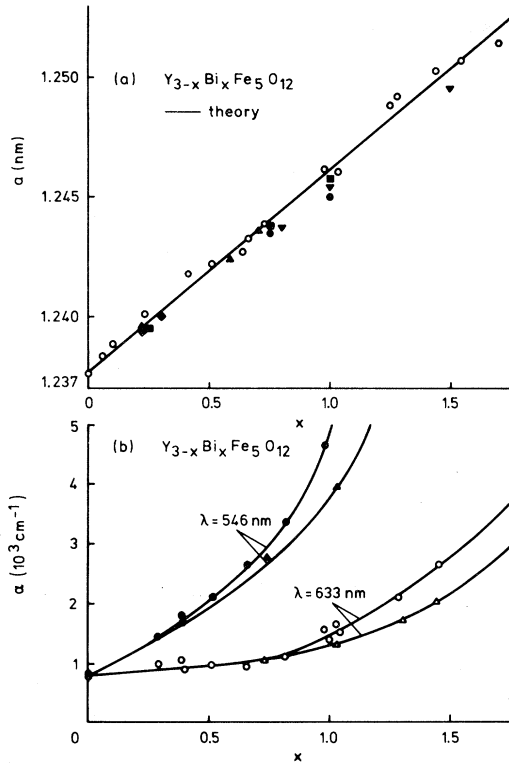
FIG. 2. Dependence of (a) the lattice constant and (b) the optical absorption on the bismuth content. The solid symbols in (a) are literature data (▼, Refs. 13,35; ◆, Ref. 18; ■, Ref. 33; ▲, Ref. 34; ●, Refs. 36,37). The solid line was calculated from the ionic radii.[30] The circles and triangles in (b) represent films grown from melts E and C, respectively.

FIG. 3. Optical absorption vs wavelength of various bismuth contents at $T=295$ K. The solid lines represent films grown from melts B and E and the dashed lines films grown from melt C.

tent x_m in these garnets is limited by the lattice constant and the lattice mismatch then it is expected to be $x_m \leq 2.2$.[22] The strong effect of lead on the optical absorption can be used as a sensitive measure to characterize the film growth. This is also reflected by the α values for the bismuth-containing samples grown from different melts as shown in Fig. 2(b). The circles represent films grown from melt E and the triangles films grown from melt C. The latter have been grown with a lower supercooling and thus contain a lower lead concentration yielding lower α values. At $\lambda=633$ nm [lower curve of Fig. 2(b)] α is not influenced by the bismuth up to $x \approx 0.8$. The weak linear increase originates from the Pb^{2+}. The nonlinear increase of α with x especially at $\lambda=546$ nm is caused by the shift of the band edge due to the bismuth as it is obvious from the wavelength dependence displayed in Fig. 3 at $T=295$ K. The curves with approximately equal x values again demonstrate the strong influence of the Pb^{2+} ions on α.

The film thickness L has been deduced from the reflection spectra[39] in the wavelength range between 1 and 2 μm using an average refractive index $\bar{n}=2.17$ for $x \leq 0.4$ and $\bar{n}=2.25$ for $x > 0.4$. The data are also summarized in Table II.

B. Magnetic properties

1. Saturation magnetization

The saturation magnetization M_s was measured with a vibrating sample magnetometer in fields up to 1.6×10^6 A m^{-1}. The M_s data are obtained from extrapolation to zero field. The accuracy of the measurements is about $\pm 1\%$, however, it is limited by the lower accuracy of the film thickness of $\pm 5\%$. The temperature dependence of the polarization $I_s = \mu_0 M_s$ is displayed in Fig. 4 for three compositions. At $T=0$ K, I_s varies between 247
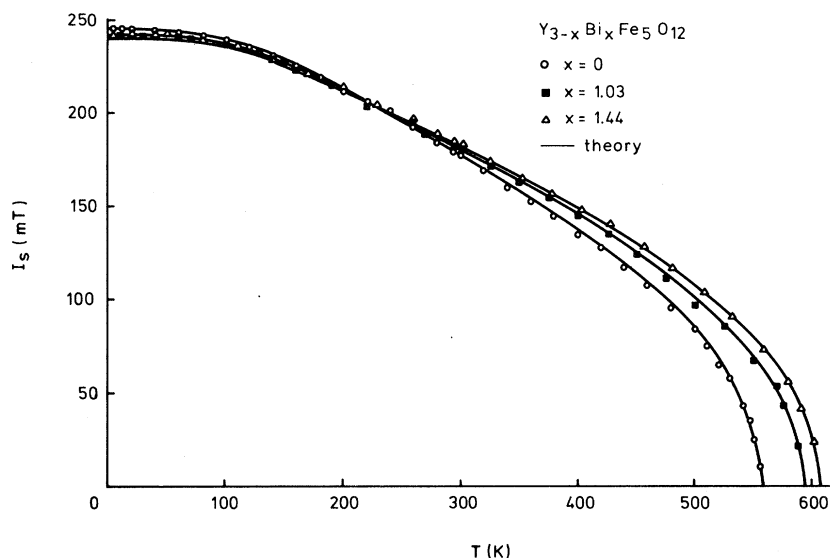
FIG. 4. Temperature dependence of the saturation polarization $I_s = \mu_0 M_s$ for different bismuth contents. The solid lines were calculated applying the molecular field theory.
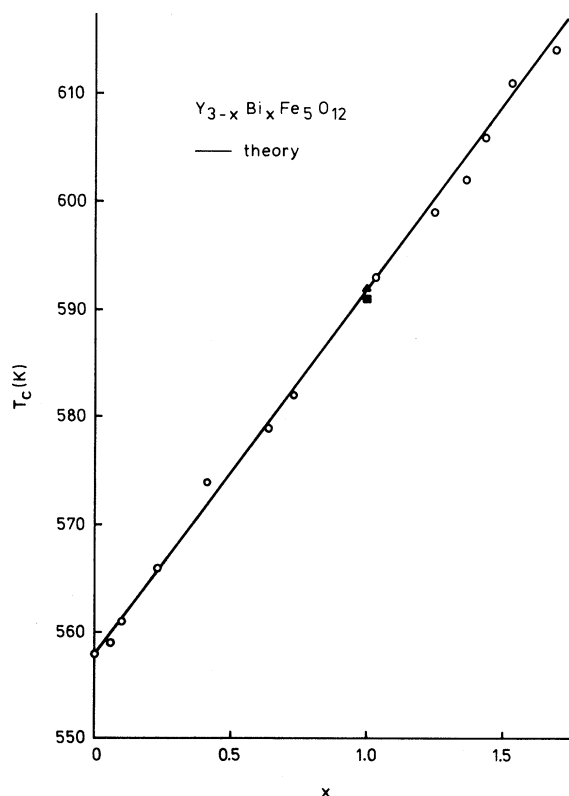
FIG. 5. Curie temperature vs bismuth content. The solid symbols refer to literature data (▲, Ref. 13; ■, Ref. 33). The solid line was calculated applying the molecular field theory.

mT $\leq I_s \leq 239$ mT for $0 \leq x \leq 1.71$. The small reduction of I_s has to be attributed to the increase of the lattice constant with increasing bismuth content. The average moment of the iron ions, however, remains unchanged within the limits of the accuracy of the experimental data. At high temperatures the average iron moment is increased by the bismuth in accordance with measurements reported for polycrystalline garnets.[33] This rise of I_s is due to the increased superexchange interaction which causes a linear increase of the Curie temperature with the Bi content as shown in Fig. 5. The change of the Curie temperature $\Delta T_C/x$ was found to be 34 K in good agreement with that for Bi-substituted gadolinium iron garnets.[22] The value $\Delta T_C/x = 38$ K reported in Ref. 33 is based on a corresponding lower T_C value for pure yttrium iron garnet. The T_C values are additionally compiled in Table III. The solid lines in Figs. 4 and 5 have been calculated from the molecular field theory and will be discussed in Sec. III A 1.

2. Anisotropy and magnetostriction

To investigate the influence of the bismuth on the cubic anisotropy constants K_i and on the magnetostriction constants $\lambda_{100}, \lambda_{111}$ spheres cut from flux-grown crystals[40] were measured applying the resonance method[41−43] at 9.2 GHz. The samples exhibit no growth-induced anisotropy. The dependence of these properties on x at $T = 295$ K is shown in Fig. 6(a) revealing a linear decrease of K_1 and λ_{111} while

TABLE III. Measured Curie temperature, Faraday rotation (at $\lambda = 633$ nm) and Faraday ellipticity (at $\lambda = 633$ or 546 nm) of some of the investigated garnet films. (a) The Pb content for the Bi-substituted films has to be considered as an impurity; (b) measured at $\lambda = 546$ nm.

| Substitution | | | $\theta_F (10^3 \ \deg \, cm^{-1})$ | | $-\psi_F (10^3 \ \deg \, cm^{-1})$ | |
x	$y^{(a)}$	T_C (K)	$T = 4.2$ K	$T = 295$ K	$T = 4.2$ K	$T = 295$ K
0	0.006	558	0.42	0.95	0.38	0.51
0	0.013	558	0.34	0.84	0.43	0.52
0	0.051	559	0.06	0.49	0.78	0.75
0	0.084	560	−0.31	0.07	1.24	1.05
0	0.143	561	−1.15	−0.60	1.81	1.32
0	0.246	562	−2.04	−1.48	2.76	2.12
0.06	0.010	559	−0.75	−0.10		1.2[b]
0.10	0.021	561	−1.85	−1.10		1.8[b]
0.24	0.044	566	−4.65	−3.65		3.0[b]
0.41	0.092	574	−8.30	−6.90		6.3[b]
0.65	0.189	579	−16.2	−12.6		
0.73	0.034	582	−16.6	−13.6		8.2[b]
1.03	0.047	593	−24.2	−19.3		12.7[b]
1.25	0.063	599	−31.0	−25.9		10.7[b]
1.44	0.080	606	−38.3	−31.7		22.0[b]
1.54	0.091	611	−40.6	−32.9		
1.71	0.130	614	−44.1	−35.8		

λ_{100} remains unchanged. In particular the solid line for λ_{111} can be represented by the relation

$$\lambda_{111}(x) = \lambda_{111}(0)(1 + 0.23x) , \qquad (1)$$

where $\lambda_{111}(0) = -2.73 \times 10^6$ according to Ref. 44. K_2 was found to be negligible for all compositions and temperatures. For films with constant x, λ_{111} can be derived from a plot of K_u vs $\Delta a^\perp / a$ yielding for films with $x = 1.03 \pm 0.05$ $\lambda_{111} = -3.4 \times 10^6$ which is in good agreement with the bulk values represented by Eq. (1). The temperature variation of λ_{100} and λ_{111} is given in Fig. 6(b). The data for $Y_3Fe_5O_{12}$ are taken from Ref. 45. These dependences again clearly demonstrate that λ_{100} is not affected by the bismuth except for the high-temperature range because of the increased Curie temperature. The temperature dependence of K_1 is shown in Fig. 7(a). It turns out that for both quantities K_1 and λ_{111} the characteristic temperature dependence of $Y_3Fe_5O_{12}$ has not been changed by the bismuth. The open squares in Fig. 7(a) represent film data.

The anisotropy of epitaxial garnet films is composed of the cubic and the uniaxial anisotropy, the latter originating from the lattice mismatch and the growth conditions. These anisotropies were measured with the resonance and the torque method. From the resonance conditions for the parallel ($\vec{M} \| [110]$) and the perpendicular ($\vec{M} \| [111]$) magnetized disks of 2 mm diameter,

$$\omega = \gamma \left[H_\perp - 4\pi M_s - \frac{4}{3} \frac{K_1}{M_s} + \frac{2K_u}{M_s} \right] , \qquad (2)$$

$$\omega^2 = \gamma^2 H_{\|} \left[H_{\|} + 4\pi M_s - \frac{K_1}{M_s} - \frac{2K_u}{M_s} \right] ,$$

the anisotropy constants can be evaluated provided the gyromagnetic ratio γ is not affected by lead or bismuth. $\omega = 2\pi f$ is the frequency ($f = 9.2$ MHz) and $H_{\|}$ and $H_\perp$ are the fields for resonance for the parallel and perpendicular magnetized film. K_2 has been neglected according to the results of the flux-grown crystals. The uniaxial anisotropy constant K_u is composed of the stress-induced part K_u^λ and the growth-induced part K_u^g:

$$K_u = K_u^\lambda + K_u^g , \qquad (3)$$

$$K_u^\lambda = -\frac{3}{2} \frac{E}{1 + \mu_{111}} \left[\frac{\Delta a^\perp}{a} \right] \lambda_{111} .$$

$\Delta a^\perp / a$, E, and μ_{111} are the relative perpendicular lattice mismatch, the Young modulus, and the Poisson constant, respectively. E and μ_{111} are related to the elastic constants C_{ik} by

$$E = (C_{11} - C_{12})(C_{11} + 2C_{12})(C_{11} + C_{12})^{-1}$$

and

$$\mu_{111} = \tfrac{1}{2}(C_{11} + 2C_{12} - 2C_{44})(C_{11} + 2C_{12} + C_{44})^{-1} .$$
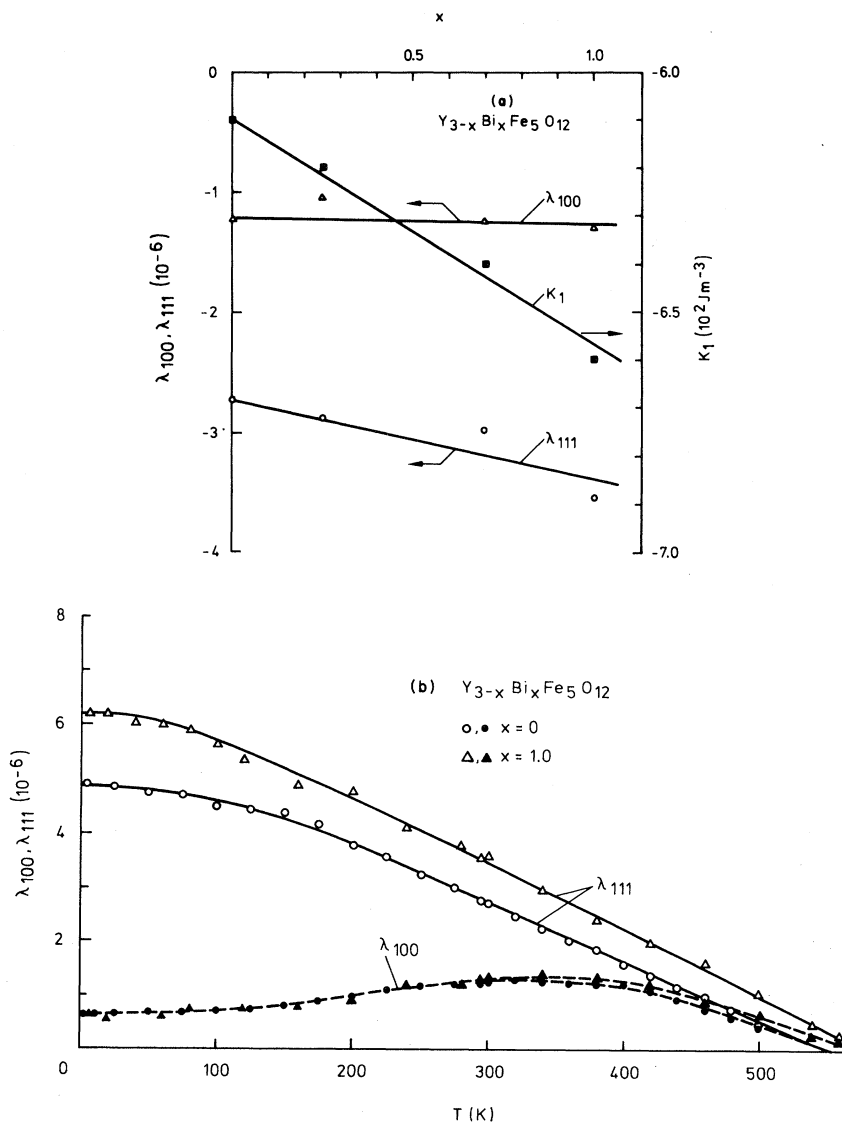
FIG. 6. (a) Concentration dependence of the magnetostriction constants λ_{100} and λ_{111} and the cubic anisotropy constant K_1 of flux-grown crystals at $T=295$ K and (b) the temperature dependence of the magnetostriction constants of flux-grown crystals.

Using the C_{ik} of $Y_3Fe_5O_{12}$ from Ref. 46, E and μ_{111} can be determined yielding 2.055×10^{11} Jm^{-3} and 0.296, respectively. With these values and those measured for $\Delta a^{\perp}/a$ and λ_{111} the stress-induced anisotropy constant K_u^{λ} can be calculated and thus also $K_u^g = K_u - 2.38 \times 10^{11}(\Delta a^{\perp}/a)|\lambda_{111}|$, provided the influence of lead and bismuth on E and μ_{111} and the temperature dependence of $\Delta a^{\perp}/a$ is negligible. The temperature dependence of K_u^g is presented in Fig. 7(a). For sample no. 13 ($x=1.03$) torque measurements were performed for $T \geq 295$ K which are represented by the encircled dots. These data

demonstrate the good agreement of the results obtained from these two measurement methods. For all compositions the convex curvature in the low-temperature range corresponds to that of the K_1 dependency. This can be interpreted in terms of the iron sublattice magnetizations in contrast to the case where mixed rare-earth ions on dodecahedral sites are the origin of K_u^g where a concave dependence of K_u^g with T has been observed.[7] The dependence of K_u^g on concentration is displayed in Fig. 7(b). Most of the data were measured with the torque method using an evaluation of the data described in Ref. 47.
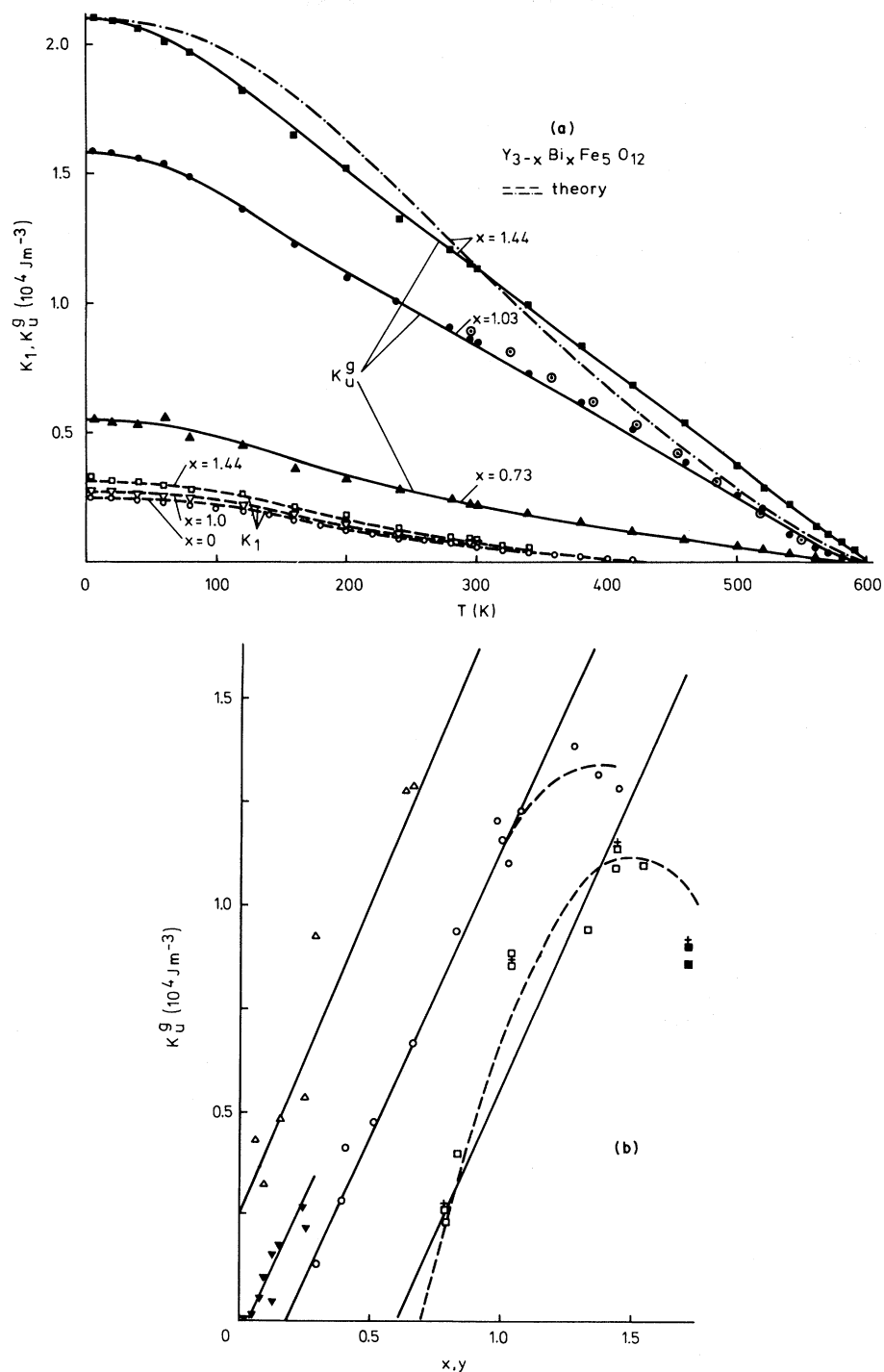
FIG. 7. (a) Temperature dependence of the cubic (open symbols) and the growth-induced anisotropy constant (solid symbols). The open circles and triangles represent data from flux-grown crystals while all other symbols refer to film data. The encircled dots are data obtained with the torque method and all other data with the resonance method at 9.2 GHz. The dashed lines and the dashed-dotted line has been calculated from the single-ion theory. (b) Dependence of the growth-induced anisotropy at $T=295$ K on the bismuth content for films grown from different melts (Δ, $\square$, $\blacksquare$, and $\bigcirc$ refer to films grown from melts B, C, D, and E, respectively). The solid triangles represent the data for films containing only lead (grown from melts A and A^*). The symbols marked with a cross are measured with the resonance method at 9.2 GHz and all other with the torque method. For the dashed lines see text.

The resonance data are marked with a cross. The data obtained with these two methods again are in good agreement. The triangles, circles, and squares represent values of films grown from the melts B, E, and C, and D, respectively. The solid triangles represent lead-substituted films grown from melts A and A^*. For each melt the growth-induced anisotropy thus roughly increases linearly with the bismuth and the lead content. For the films grown from melt C and E, Bi contents above $x=1$ have been achieved and these samples indicate a reduction of K_u^g with higher x values. In that case a variation as expected from the site ordering model [dashed line in Fig. 7(b)] leads to a better description of the ex-

perimental data. This aspect will receive further consideration in Sec. III.

C. Magneto-optic properties

1. Lead-substituted films

The Faraday rotation θ_F and the Faraday ellipticity $\epsilon_F = \tanh(\psi_F L)$ are strongly affected by the lead incorporation,[17,21,23,24] where the Pb^{2+} ion plays the dominant role.[23,24] The dependence of θ_F and ψ_F expressed in $\deg \, cm^{-1}$ vs Pb concentration at $T=295$ K and $\lambda=633$ nm is shown in Fig. 8. Both θ_F and ψ_F exhibit a linear variation with Pb (dashed lines) and Pb^{2+} (solid lines) content. The triangles
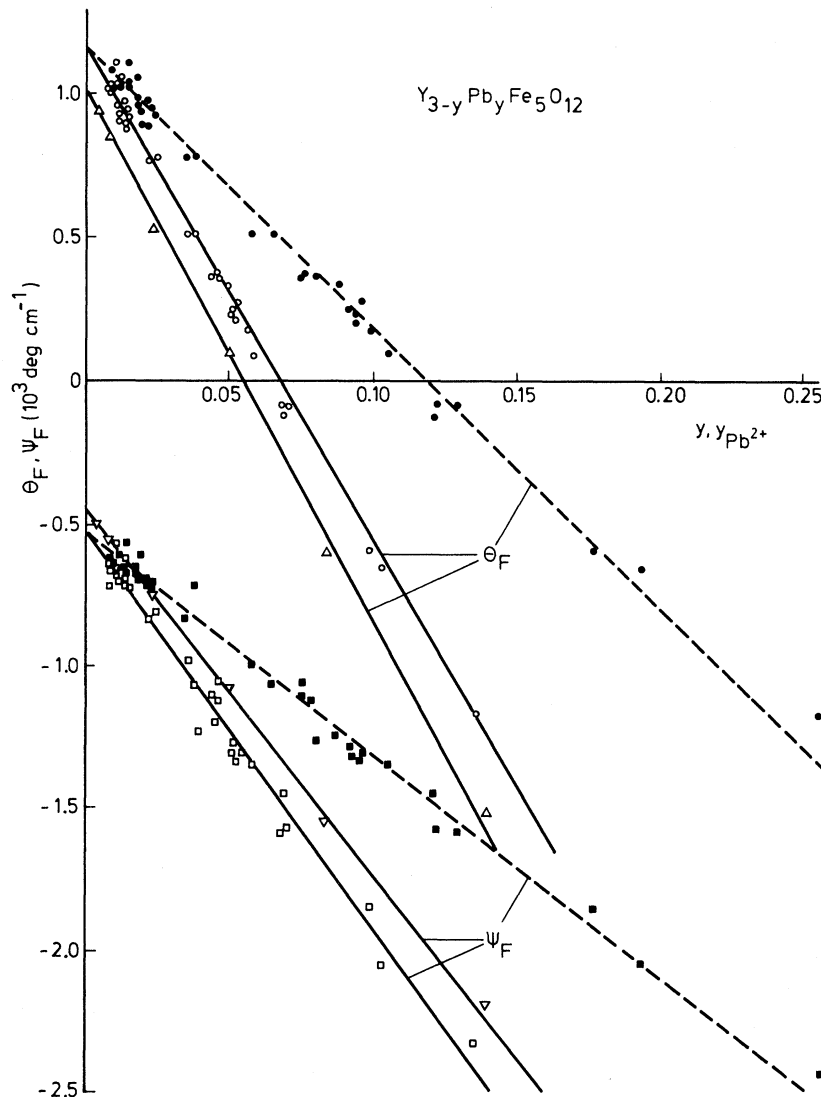
FIG. 8. Dependence of the Faraday rotation θ_F and Faraday ellipticity ψ_F on the total lead content y (dashed lines) and the Pb^{2+} content $y_{Pb^{2+}}$ (solid lines) at $\lambda=633$ nm and $T=295$ K. The triangles refer to films grown from melt A and the circles and squares to films grown from melt A^* ([Fe]/[Y] > 12).

refer to films grown from melt A and the circles and squares, refer to films grown from melt A^* ([Fe]/[Y] > 12). For $Gd_{3-y}Pb_yFe_5O_{12}$ films this linear dependence of ψ_F on Pb^{2+} content occurs at shorter wavelengths.[24]

From extrapolation to zero lead content θ_F and ψ_F of a lead-free $Y_3Fe_5O_{12}$ crystal at $\lambda = 633$ nm can

be determined which yields at $T = 4.2$ K, $\theta_F = 560$ deg cm^{-1} and $\psi_F = -240$ deg cm^{-1} and at $T = 295$ K, $\theta_F = 980$ deg cm^{-1} and $\psi_F = -410$ deg cm^{-1}. The contributions $\Delta\theta_F/y$ and $\Delta\psi_F/y$ for the films grown from melt A (triangles in Fig. 8) at $T = 4.2$ K were found to be $-18\,500$ deg cm^{-1} and $-18\,200$ deg cm^{-1} and at $T = 295$ K were $-18\,400$ deg cm^{-1}
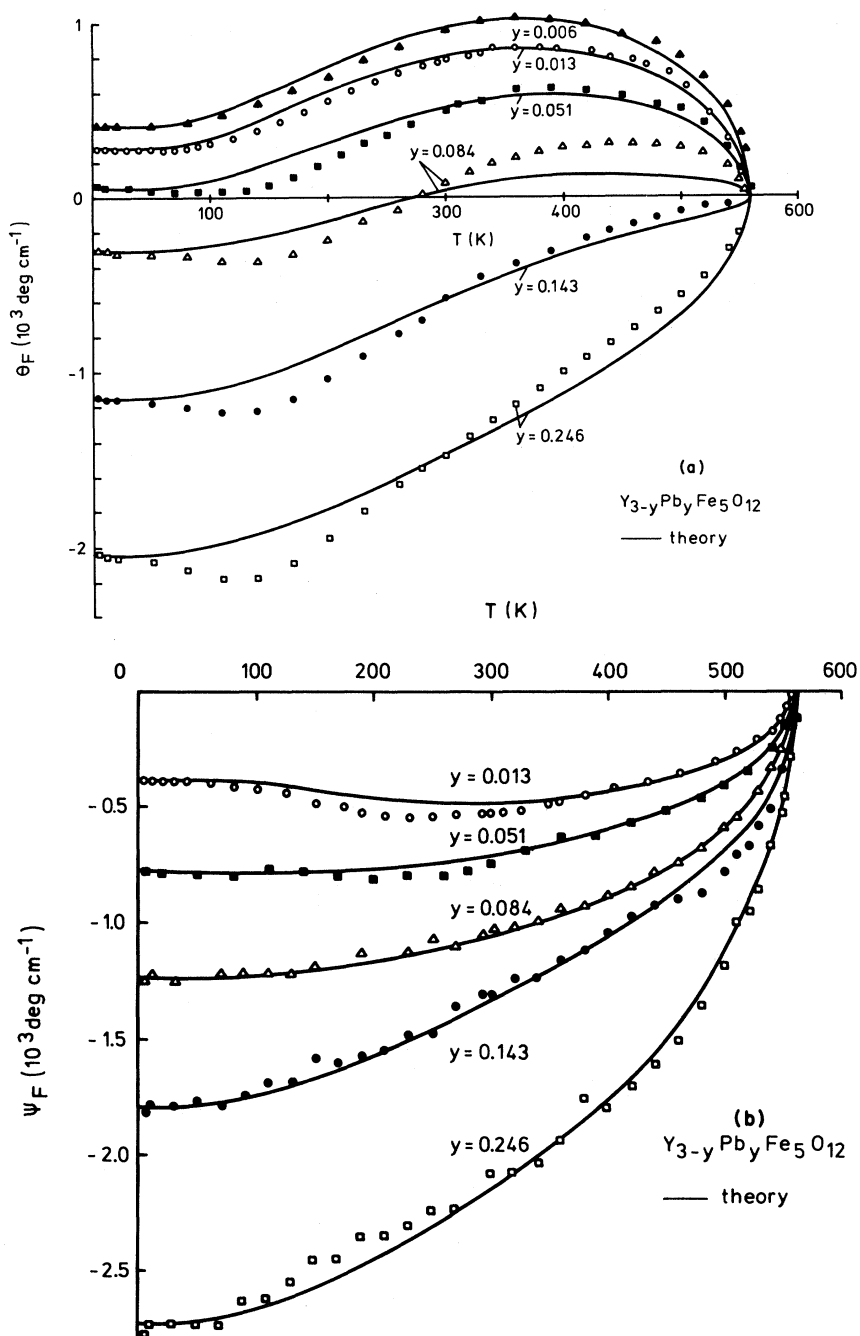
FIG. 9. Temperature dependence of (a) the Faraday rotation and (b) the Faraday ellipticity at $\lambda = 633$ nm for various lead contents.

and $-12\,600$ degcm^{-1}, respectively. The films grown from melt A^* (squares and circles in Fig. 8) lead to slightly different values reflecting the influence of the growth conditions in particular for $y=0$. These considerably higher contributions of the lead to θ_F and ψ_F as compared to the Pb-substituted gadolinium iron garnets[23,24] explain the scatter of the θ_F and ψ_F data found for different $Y_3Fe_5O_{12}$ samples. The lead content usually ranges between $0.005 \leq y \leq 0.020$ which is related to supercoolings between 3 K $\leq \Delta T_s \leq 20$ K and thus causes a scatter of θ_F at $T=4.2$ K within the limits $200 \lesssim \theta_F \lesssim 450$ degcm^{-1}. A corresponding spread occurs for ψ_F. The problem arising from the scatter of θ_F and ψ_F already has been discussed in a recent work on $Y_3Fe_{5-x}Ga_xO_{12}$ garnet films[48] but could not be explained there satisfactorily, since lower Pb^{2+} contributions had been assumed.

The temperature dependences of θ_F and ψ_F are displayed in Figs. 9(a) and 9(b). For θ_F a minimum around 100 K is induced by the lead, as was also found for $Gd_{3-x}Pb_xFe_5O_{12}$ films.[24] Thus it seems to be correlated to the iron sublattices and not necessarily to the dodecahedral sublattice. The solid lines

were calculated on the basis of the sublattice magnetizations and will be discussed in Sec. III. The θ_F and ψ_F data for $T=4.2$ K and $T=295$ K are also compiled in Table III.

2. Bismuth-substituted films

The dependence of θ_F on bismuth concentration x at $\lambda=633$ nm is shown in Fig. 10(a). The crosses are data from literature.[18,19] The dependence for $Gd_{3-x}Bi_xFe_5O_{12}$ films (dashed lines)[22] is given for comparison and demonstrates that the magneto-optical behavior of the bismuth is very similar in these hosts. The contributions $\Delta\theta_F/x$ at $T=4.2$ and 295 K are $-25\,400$ and $-20\,600$ degcm^{-1}, respectively. The Bi-induced ellipticity at $\lambda=633$ nm is negligibly small as was shown for the absorption α. The triangles and circles represent data for films grown from the melts B and E, respectively. They exhibit no significant difference in the magneto-optical behavior at this wavelength in contrast to shorter wavelengths. The corresponding plots of θ_F at $\lambda=546$ nm and 589 nm and ψ_F at $\lambda=546$ nm vs
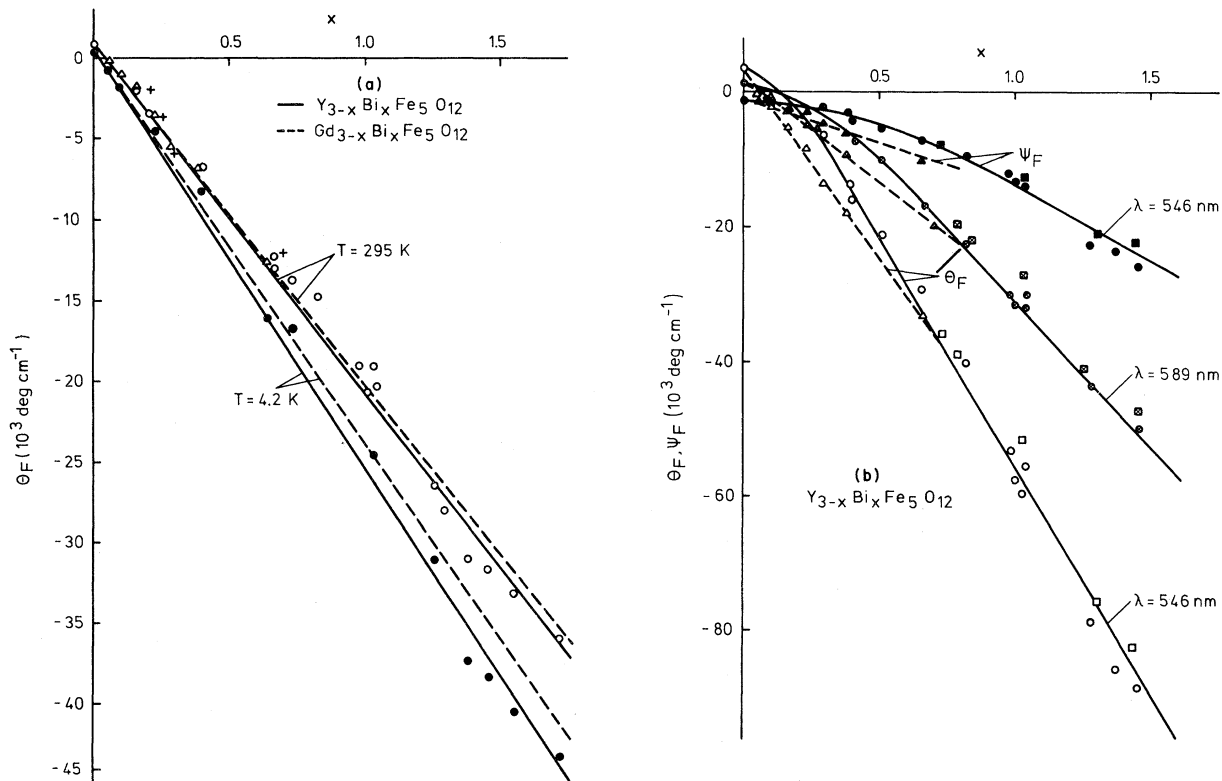
FIG. 10. Dependence of the Faraday rotation on the bismuth content (a) at $\lambda=633$ nm and (b) the Faraday rotation at $\lambda=546$ and 589 nm and ellipticity at 546 nm for $T=295$ K. The triangles, squares, and circles represent data for films grown from melts B, C, and E, respectively. The crosses in (a) represent literature data.[18,19]
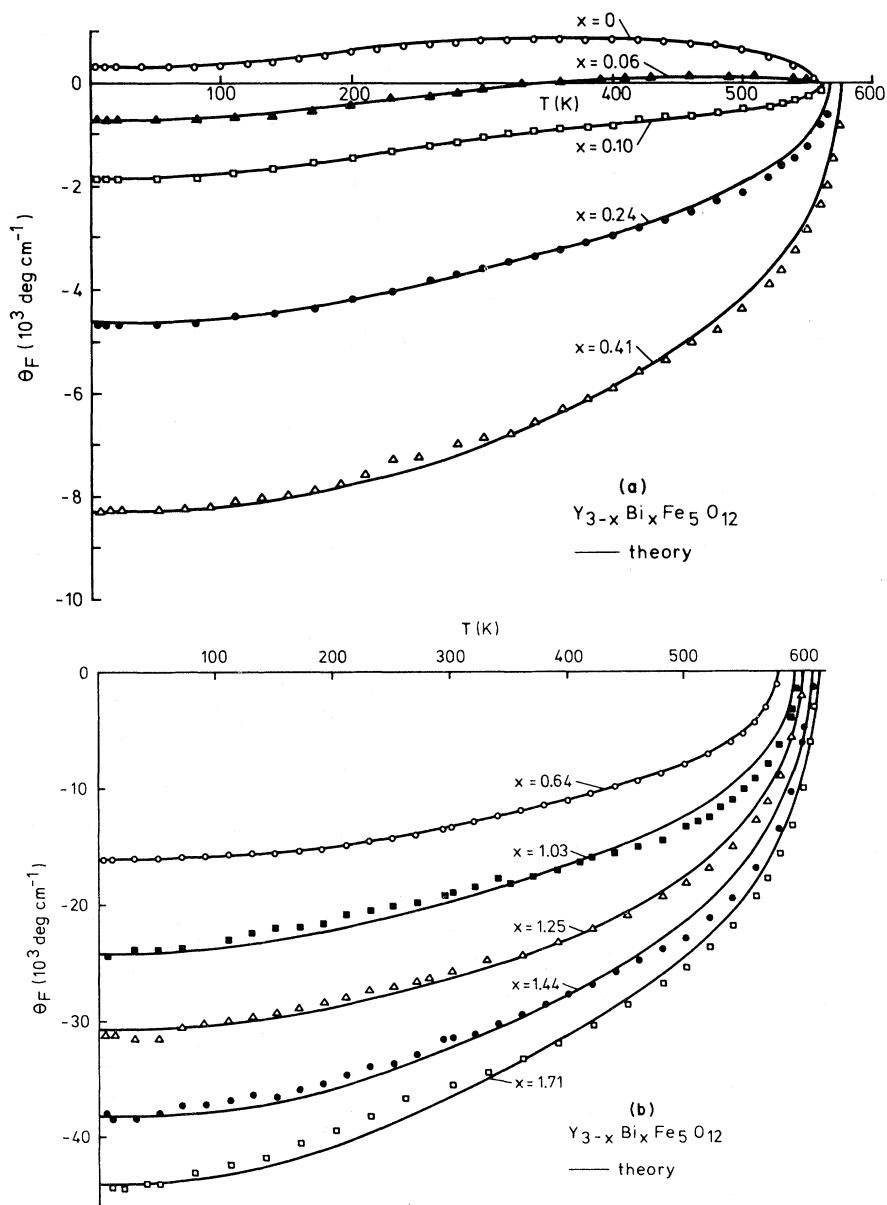
FIG. 11. Temperature dependence of the Faraday rotation at $\lambda = 633$ nm for various bismuth concentrations.

x shown in Fig. 10(b) indicate a slight difference for these films. The data of the films grown from melt C (squares) agree with those from melt E (circles). The films grown from melt B exhibit lower θ_F and ψ_F values. The separations of the θ_F values, e.g., at $x = 0.3$ is about 6000 deg cm^{-1} while the actual difference of the lead content at most would cause a difference of 1000 deg cm^{-1}. For ψ_F the separation is smaller but still too large to be explained by the different Pb contents alone. This difference which also occurs at other wavelengths thus seems to reflect different growth conditions. The films from

melt B are grown with lower growth rates than those from melts C and E.

The temperature dependence of the Faraday rotation at $\lambda = 633$ nm is displayed in Figs. 11(a) and 11(b). The solid lines represent the calculated dependences based on the sublattice magnetizations and will be discussed in Sec. III.

The figure of merit $2 \mid \theta_F \mid /\alpha$ can be determined from the data of θ_F and α. This quantity is of high interest for magneto-optical device applications. The variation of $2 \mid \theta_F \mid /\alpha$ vs x is shown in Fig. 12 for two wavelengths. A typical maximum occurs
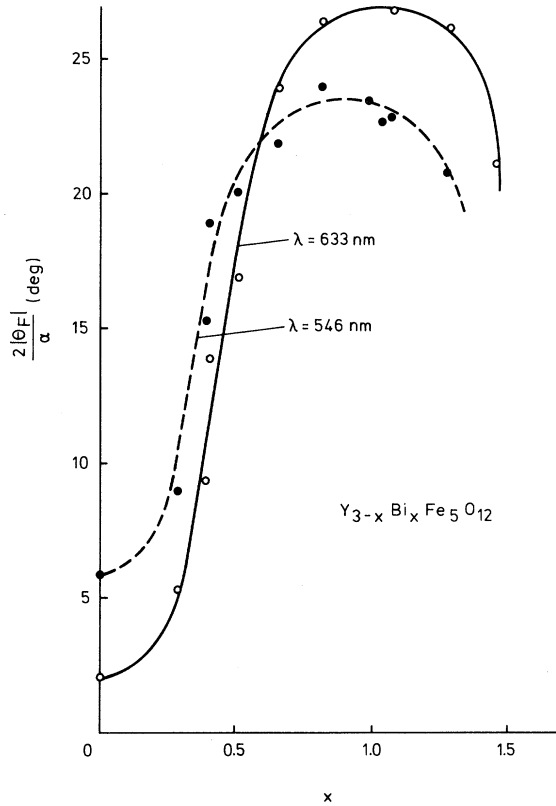
FIG. 12. Figure of merit $2\,|\,\theta_F\,|\,/\alpha$ vs bismuth content at $T=295$ K.

between $0.8 \leq x \leq 1.1$ originating from the shift of the band edge together with the increasing Pb content as it is also observed for Bi-substituted gadolinium and samarium iron garnets.[22,49] At $\lambda = 589$ nm a slightly higher maximum value of 33° was found as compared to 24° and 27° obtained for $\lambda = 546$ and 633 nm, respectively.

III. DISCUSSION

A. Magnetic properties

1. Saturation magnetization

The saturation magnetization of ferrimagnetic garnets can be well described by the molecular field theory.[21,50,51] To account for the influence of the bismuth on the superexchange interaction[33,35,38] and thus on the Curie temperature, the molecular field constants N_{aa}, N_{dd}, and N_{ad} of pure $Y_3Fe_5O_{12}$ given in Ref. 51 must be modified according to the relation

$$N_{ik}(x)=N_{ik}(0)(1+\delta_{ik}x) \,, \qquad (4)$$

where $\delta_{ik} \approx [1/T_C(0)]dT_C/dx$ and $i,k =a,d$ refer to the octahedral (a) and tetrahedral (d) sublattice. The concentration and temperature dependence of M_s and the concentration dependence of T_C have been calculated with $\delta_{aa}=\delta_{dd}=0$ and $\delta_{ad}=0.032$ (solid lines in Figs. 4 and 5) yielding a good fit to the experimental data. This value of δ_{ad} is in agreement with that used for $Gd_{3-x}Bi_xFe_5O_{12}$ films where $\delta_{ad}=0.035$.[21,22] A calculation of the δ_{ik} on the basis of the microscopic models proposed to explain the origin of the bismuth-induced effects is not yet possible. The calculated curves imply an increasing average impurity content of lead and platinum inferred from the analysis data given in Table II. From this calculation the temperature dependence of the sublattice magnetizations M_a and M_d are available which are necessary to describe the temperature behavior of the anisotropy constants and the magneto-optical properties.

2. Cubic anisotropy and magnetostriction

Different mechanisms have been proposed to explain the strong influence of the bismuth on the superexchange interaction, the "structural" model[38,52] and the "electronic" model.[14,49] The first model assumes a more favorable interaction geometry of the iron and oxygen ions because of the induced distortion by the bismuth ions. This indeed will affect the superexchange interaction, however, the influence on the spin-orbit coupling, which is important for the anisotropy and magnetostriction, is expected to be small. The magneto-optical effects, however, indicate that a pronounced increase of the effective spin-orbit coupling of the mixed oxygen-iron states involved in the optical transition is present via mixing of $6p$ orbitals of the bismuth.[14] This should be reflected in the magnitude of the anisotropy and magnetostriction constants. The concentration and temperature dependence, indeed, can be regarded as a further evidence that the bismuth-induced effects are not only structural in origin. The cubic anisotropy constant K_1 can be expressed in terms of the single-ion model[53] by the relation

$$K_1(T)= \sum_{p=a,d} N_p[u_p r_p(y_p)+v_p t_p(y_p)] \,,$$

$$y_p =\exp\left[-\frac{g\mu_B H_{\text{exch}}^{(p)}}{kT}\right] \,, \qquad (5)$$

where g, μ_B, and k are the g factor, the Bohr magneton, and the Boltzmann constant. N_a and N_d denote the number of Fe^{3+} ions on octahedral and tetrahedral sites per cm^{-3}, respectively. u_p is related to the spin-orbit coupling constant λ_{so} by $u_p \sim \lambda_{\text{so}}^4$

and v_p to the exchange field $H_{exch}^{(p)}$ by $v_p \sim (H_{exch}^{(p)})^{-1}$. The functions $r_p(y_p)$ and $t_p(y_p)$ govern the sublattice temperature behavior where at $T=0$ K $r_p(y_p)=t_p(y_p)=1$. The second term of Eq. (5) is small and can be neglected for $Y_3Fe_5O_{12}$. Thus the substitution of bismuth is not expected to change K_1 at $T=0$ K provided the bismuth only affects $H_{exch}^{(p)}$. The experimental data (from bulk crystals and films) clearly exhibit a significant linear increase of $|K_1|$ at $T=0$ K which can be attributed to a rise of λ_{so} or to an increase of the second term of Eq. (5) because of the much larger single-ion contribution of the distorted iron ions which, however, is expected to be cancelled out for a random distribution of these ions over the nonequivalent a and d sites. The temperature dependence of K_1 can be well described by Eq. (5) for all Bi concentrations [dashed lines in Fig. 7(a)] where the second term of Eq. (5) has been neglected. The sublattice magnetizations controlling $H_{exch}^{(p)}$ and thus y_p were inferred from the fit of the molecular field theory to the measured saturation magnetization as treated in Sec. A 1. At high temperatures, both the increased λ_{so} and $H_{exch}^{(p)}$ tend to increase K_1 as observed [Fig. 6(a)]. The increase of the effective spin-orbit coupling is also confirmed by the increased magnetostriction constant λ_{111} [Figs. 6(a) and 6(b)].

3. Uniaxial anisotropy

Large uniaxial anisotropies have been observed for bismuth-substituted iron garnets[6,8,9,22] where the stress-induced part is well understood in terms of Eq. (3). The growth-induced part, however, has not yet been explained satisfactorily. Since it increases linearly with the Bi content for each melt [Fig. 7(b)], it is expected to originate either from an ordering of the Bi and Y ions on dodecahedral sites or from an ordering of defects or impurities associated with the bismuth and entering the crystal proportional to x. In both cases the distortion of the environment of the Fe^{3+} ions with respect to the ordering process must be responsible for the large uniaxial anisotropies similar to the case described for other diamagnetic substituents in iron garnets.[54] For the case that an ordering of the Bi ions takes place a concentration dependence of $K_u^g(x)$ of the form $K_u^g(x)=K_u^g(0)x(3-x)$ is expected according to the preferential site ordering model[55] and such a dependence indeed was found for $Y_{3-x}Lu_xFe_5O_{12}$ garnets.[56] To confirm this relation the x values should be significantly larger than $x_m=1.5$ where the maximum of $K_u^g(x)$ occurs. Unfortunately the maximum Bi content attainable for the investigated films was $x=1.7$. Therefore, it will be difficult to decide whether a Bi site ordering or an ordering of

defects or impurities leading to a linear dependence up to higher x values is present. The data presented in Fig. 7(b) indicate a linear dependence for films grown from melt B ($x \lesssim 1$). Higher x values have been realized for the films grown from melts C, E, and D. In this case a dependence of the form $K_u^g(x)=K_u^g(0)(x-x_0)(3-x_0-x)$ with, e.g., $x_0=0.6$ (corresponding to squares) leads to a better description [dashed line in Fig. 7(b)] of the experimental data than a linear dependence on x. Further, the experimental results show that a threshold x_0 for the ordering process seems to be present where x_0 depends on the growth conditions.

The temperature dependence of K_u^g is expected to be described by an equation similar to Eq. (5) provided the single-ion anisotropy is the origin of this quantity. In contrast to K_1 the iron ions contributing to K_u^g are strongly distorted by the Bi ions and therefore the second term of Eq. (5) will be the dominant one. Possibly even higher-order terms in the Hamiltonian have to be considered.[54] This is reflected in the temperature dependence of K_u^g which reduces much less with T and is even almost linear in a wide range of temperatures while K_1 drops much faster. This is not obvious from Fig. 7(a) since $K_1 \ll K_u^g$ but from a plot of $K_1(T)/K_1(0)$ and $K_u^g(T)/K_u^g(0)$ vs T this feature becomes clearly evident. This implies that the first term of Eq. (5) fails to account for the temperature variation of K_u^g while the second term decreases much more slowly with T and qualitatively agrees with the experimental data (sample no. 15) as shown by the dashed-dotted line in Fig. 7(a). To improve the agreement between theory and experiment the correct temperature dependence for K_u^g has to be calculated since Eq. (5) applies to the cubic case. For a nonrandom distribution of the distorted iron ions over the nonequivalent a and d sites K_u^g can be determined analogous to K_1 from the free energy $F(hkl)$ evaluated at particular crystallographic directions $[hkl]$ by

$$K_u^g=3[F(100)-F(110)] ,$$

$$F(hkl)=-kT \sum_{p=a,d} N_p \sum_{i=1}^{n_i(p)} \frac{\ln Z_i^{(p)}}{n_i(p)} ,$$
(6)

where $Z_i^{(p)}$ is the partition function which is related to the energy levels $E_j(\gamma_i^{(p)})$,

$$Z_i^{(p)} = \sum_j \exp\left[-\frac{E_j(\gamma_i^{(p)})}{kT}\right]$$
(7)

at octahedral ($p=a$) and tetrahedral ($p=d$) sites. N_a and N_d now denote the total number of distorted iron ions on a and d sites, respectively. $n_i(p)$ is the number of the nonequivalent sites and γ_i the angle between the local axis of distortion and the direction

of magnetization. The calculation of K_u^g thus requires the knowledge of the quantities $n_i(p)$, $\gamma_i^{(p)}$, and $E_j(\gamma_i^{(p)})$ where the latter have been given in Ref. 53. The numbers $n_i(p)$ essentially determine the magnitude of K_u^g and the angles γ_i control the temperature variation. The $n_i(p)$ have been discussed for dodecahedral site ordering of diamagnetic ions,[54,55] however, the local axes of distortion on a and d sites which determine the $\gamma_i^{(p)}$ have not been investigated. The nearest d sites with respect to the dodecahedral sites will experience an enlarged distortion along the [100] directions but in the case of the next nearest d sites and the a sites the situation is more complicated. This point needs further consideration in order to calculate the temperature dependence of K_u^g in terms of the single-ion theory and thus to improve the agreement between the experiment and this theory.

Further, the problem concerning the relation between the $n_i(p)$ and the growth conditions has to be solved. This, in particular, applies to the question

whether a site ordering of the bismuth or an ordering of defects or impurities associated with the incorporation of the bismuth in the crystal causes K_u^g. This cannot yet be decided on the basis of the present experimental data. The platinum, present as an impurity, can be excluded in this respect because even in the high spin state where this ion is strongly anisotropic on a sites, the comparison of the samples 5, 11, 12, 13, and 16 with the same Pt content shows that very different growth-induced anisotropies occur. From the magnitude of K_u^g of the bismuth-free samples and the dependence of K_u^g vs Pb^{2+} or Pb^{4+} content of the bismuth-substituted samples it can be concluded that also the lead cannot be the primary origin for K_u^g in the bismuth-substituted films. Since the concentration of other impurities is much lower than that of the Pt and Pb ions presumably only the ordering of defects can be considered as a possible alternative to the ordering of the Bi ions.

The lead-substituted films indicate that the magnitude of K_u^g is comparable to the bismuth films [solid triangles in Fig. 7(b)]. In this case an ordering of Pb^{2+} and Pb^{4+} ions on dodecahedral sites can occur but also the Pb^{4+} presumably entering octahedral sites can participate in this process.

The investigation of the influence of the growth conditions on K_u^g reveal that K_u^g primarily is controlled by the supercooling. This is demonstrated in Fig. 13 presenting the K_u^g values at $T=295$ K vs ΔT_s (solid line) for films grown from different melts. K_u^g essentially increases from the origin linearly with ΔT_s where the rate of rotation was kept constant for all films investigated except for the film represented by the triangle at $x=0.29$ in Fig. 7(b) indicating that the rotation rate is a further important parameter.[57] The K_u^g data for the films grown from melt C (squares) are slightly lower and can be represented more accurately by the dashed line. This shows that further parameters such as the growth rate and the cation concentrations are of lesser importance for K_u^g than the supercooling and the rotation rate. It should be noticed that a comparison of the plots of K_u^g vs x [Fig. 7(b)] and vs ΔT_s (Fig. 13) reveal a dependence of K_u^g on both ΔT_s and the magnitude of the Bi content or a corresponding defect concentration. At $\Delta T_s=0$ different Bi contents can be realized which depends on the melt composition and determines the value of x_0 [see Fig. 7(b)]. Since at low ΔT_s the growth rate is small a more uniform distribution of the Bi ions is expected and thus also low K_u^g values as observed.

For the Pb-substituted films the data points also reveal a linear dependence on ΔT_s with a much lower slope.

Further investigations are necessary to establish
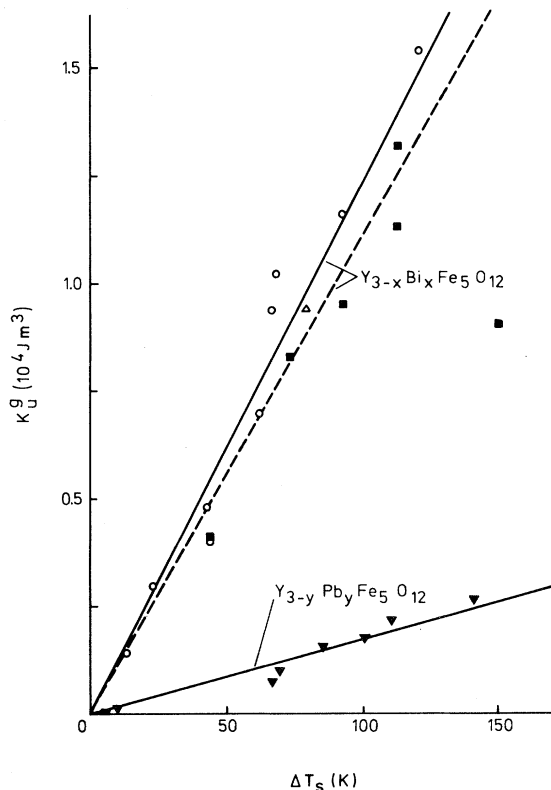
FIG. 13. Growth-induced anisotropy constant at $T=295$ K vs supercooling for lead- and bismuth-substituted yttrium iron garnet films. The symbols $\triangle$, $\square$, $\blacksquare$, $\bigcirc$, and $\blacktriangledown$ refer to films grown from melts B, C, D, E, and A,A^*, respectively.
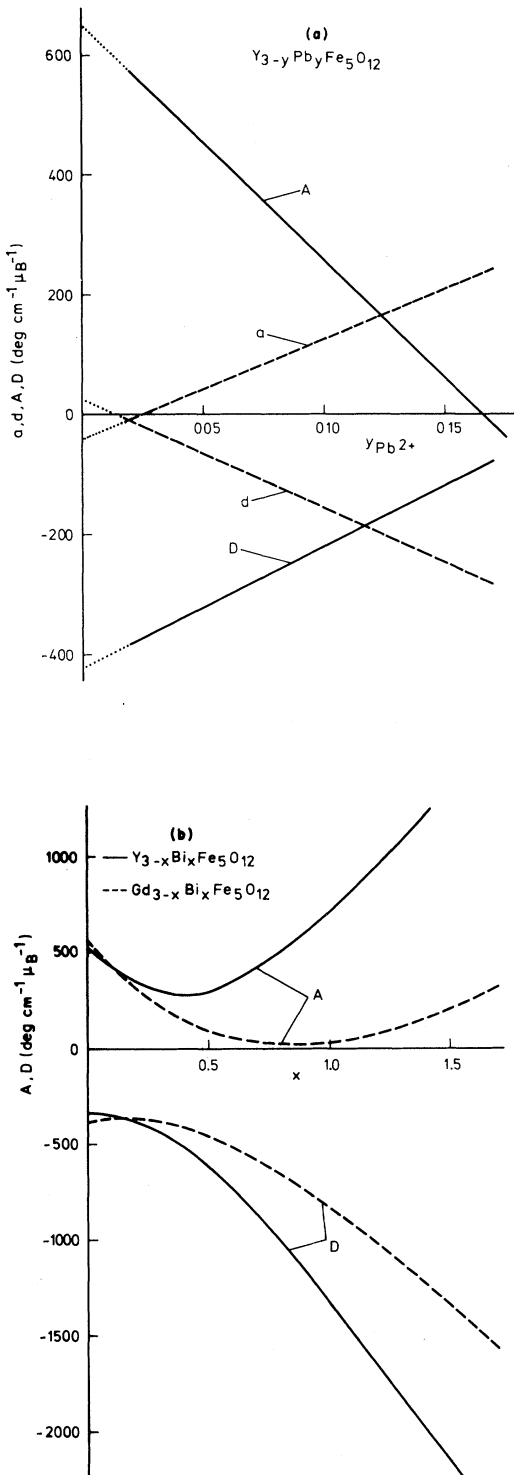
FIG. 14. Magneto-optical coefficients at $\lambda = 633$ nm vs (a) the lead content and (b) the bismuth content for bismuth-substituted yttrium and gadolinium iron garnet (Ref. 22) films.

these dependences of K_u^g on the growth parameters and to find a correlation to the ordering process. Then a more reliable discussion about the number of distorted iron ions and their local axes of distortion can be made which may lead to an improved treatment of the single-ion calculation.

B. Magneto-optical properties

The spectral dependence of the magneto-optical effects have been discussed in detail in literature.[12,13,14,19,37] Our results are in good agreement with the published work and therefore should not be presented again. We thus will restrict our considerations to the temperature dependence of the Faraday rotation and the Faraday ellipticity which can be expressed by[24,58]

$$\theta_F(T) = AM_a(T) + DM_d(T) ,$$

$$\psi_F(T) = aM_a(T) + dM_d(T) ,$$

(8)

where a,A and d,D are the magneto-optical coefficients depending on frequency. With the sublattice magnetizations inferred from the fit of the molecular field theory to the measured saturation magnetization $\theta_F(T)$ and $\psi_F(T)$ can be calculated where the magneto-optical coefficients were determined by adjustment of $\theta_F(T)$ and $\psi_F(T)$ at two temperatures. For the lead-substituted films the calculated dependence for θ_F at $\lambda = 633$ nm only is in qualitative agreement with the experimental data while for ψ_F a good fit of the experimental data can be achieved [solid lines in Figs. 9(a) and 9(b)]. The occurring discrepancies are essentially caused by the minimum of θ_F appearing at low temperatures as already observed in the case of $Gd_{3-x}Pb_xFe_5O_{12}$ films.[23,24] This seems to be a typical feature of lead-substituted garnets. Whether this discrepancy has to be attributed to a temperature dependence of the coefficients A and D or to the neglection of higher-order terms in Eq. (8) (Ref. 48) cannot yet be decided on the basis of the present results.

The calculated temperature dependence of θ_F for the bismuth-substituted films at $\lambda = 633$ nm exhibits a satisfactory agreement with the experimental results [solid lines in Figs. 11(a) and 11(b)]. The small deviations from the experimental data at high temperatures indicate that higher-order terms have to be taken into account.[48] For these films ψ_F at $\lambda = 633$ nm corresponds to that of $Y_3Fe_5O_{12}$ with a certain Pb^{2+} content and therefore a comparison between experiment and theory is not meaningful.

From the temperature variations the magneto-optical coefficients can be deduced. Since the evaluation of these coefficients is very sensitive to a small scatter of the experimental data a linear inter-

polation through the experimental data at $T=4.2$ and 400 K is used. The results are shown in Figs. 14(a) and 14(b). For the lead-substituted films the coefficients vary linearly with the Pb^{2+} content within the limited range of available Pb^{2+} concentrations. In particular, A and $|D|$ are strongly reduced by the lead while the opposite behavior is present for $|a|$ and $|d|$ where the latter result is not in accordance with that found for lead-substituted gadolinium iron garnets.[24] For the bismuth containing films a nonlinear variation occurs (solid lines) similar to that of $Gd_{3-x}Bi_xFe_5O_{12}$ garnets[22] (dashed lines). These concentration dependences again indicate that the linear theory [Eq. (8)] is insufficient to describe these effects.

IV. CONCLUSION

The influence of lead and bismuth on the magnetic properties M_s, T_C, K_1, K_u, λ_{100}, and λ_{111} of epitaxial garnet films of composition $Y_{3-x}Bi_xFe_5O_{12}$ and $Y_{3-y}Pb_yFe_5O_{12}$ have been investigated as a function of temperature and concentration. The experimental results reveal a linear variation of these properties with the bismuth caused by its strong effect on the superexchange interaction and on the spin-orbit coupling. The temperature dependences can be interpreted in terms of the molecular field theory and the single-ion theory. The growth-induced anisotropy is found to depend linearly on the supercooling at constant rate of rotation for both the lead- and bismuth-substituted films and the influence of the other growth parameters appears to be of minor importance.

Further, the optical absorption α and the magneto-optical properties θ_F and ψ_F of these films have been studied. The contributions of the Pb^{2+} and Bi^{3+} ions to θ_F turn out to be of comparable magnitude. In particular, at $\lambda=633$ nm and $T=295$ K $\Delta\theta_F/x$ and $\Delta\theta_F/y_{Pb^{2+}}$ were found to be $-20\,600$ and $-18\,400$ deg cm^{-1}, respectively. The temperature dependence of θ_F and ψ_F was described in terms of the sublattice magnetizations inferred from the fit of the molecular field theory to the measured saturation magnetization. The extracted magneto-optical coefficients at $\lambda=633$ nm are temperature-independent and exhibit a linear dependence on the Bi and Pb^{2+} content for $x,y_{Pb^{2+}} \lesssim 0.2$ and a nonlinear dependence for $x > 0.2$.

[1]D. E. Lacklison, G. B. Scott, D. A. Giles, J. A. Clarke, R. F. Pearson, and J. L. Page, IEEE Trans. Magn. 13, 973 (1977).

[2]B. Hill and K.-P. Schmidt, Philips. J. Res. 33, 211 (1978).

[3]B. Hill and K.-P. Schmidt, SID J. 10, 80 (1979).

[4]W. E. Ross, D. L. Cox, J. J. Fernandez, and R. Pulliam, SID Digest, VIII, 98 (1982).

[5]B. Hill and K.-P. Schmidt, in Conference Proceedings of the Congress on Advances in N-Impact Printing Technologies, Venice, 1981, edited by J. Gaynor (van Nostrand-Reinhold, New York, 1982), p. 334; Electron Components Applications 4, 169 (1982).

[6]J. M. Roberston, H. A. Algra, and D. J. Breed, J. Appl. Phys. 52, 2338 (1981).

[7]R. C. LeCraw, L. C. Luther, and E. M. Gyorgy, J. Appl. Phys. 53, 2481 (1982).

[8]L. C. Luther, R. C. LeCraw, and F. Ermanis, J. Cryst. Growth 58, 95 (1982).

[9]L. C. Luther, R. C. LeCraw, J. F. Dillion, Jr., and R. Wolfe, J. Appl. Phys. 53, 2478 (1982).

[10]J. J. Krebs, W. G. Maisch, G. A. Prinz, and D. W. Forester, IEEE Trans. Magn. 16, 1179 (1980).

[11]G. B. Scott and D. E. Lacklison, IEEE Trans. Magn. 12, 292 (1976).

[12]Magneto-optic data are compiled by P. Hansen, K. Enke, and G. Winkler, in Landolt-Börnstein: Numerical Data and Functional Relationships in Science and Technology, Part: Iron Garnets, edited by K.-H. Hellwege (Springer, Berlin, 1977), Series 12a, p. 167.

[13]S. Wittekoek and T. J. A. Popma, J. Appl. Phys. 44, 5560 (1973).

[14]S. Wittekoek, T. J. A. Popma, J. M. Robertson, and P. F. Bongers, Phys. Rev. B 12, 2777 (1975).

[15]H. Takeuchi, K. Shinagawa, and S. Taniguchi, Jpn. J. Appl. Phys. 12, 465 (1973).

[16]K. Shinagawa and S. Taniguchi, Jpn. J. Appl. Phys. 13, 1663 (1974).

[17]K. Shinagawa, H. Takeuchi, and S. Taniguchi, Jpn. J. Appl. Phys. 12, 466 (1973).

[18]E. V. Berdennikova, R. V. Pisarev, and R. A. Petrov, Izv. Akad. Nauk. SSSR, Ser. Fiz. 35, 1081 (1971) [Bull. Acad. Sci. USSR, Phys. Ser. 35, 6 (1971)].

[19]D. E. Lacklison, G. B. Scott, H. I. Ralph, and J. L.

Page, IEEE Trans. Magn. 9, 457 (1973).

[20]D. Mateika, R. Laurien, and C. H. Rusche, J. Cryst. Growth 56, 677 (1982).

[21]P. Hansen, H. Heitmann, and K. Witter, Phys. Rev. B 23, 6085 (1981).

[22]P. Hansen, K. Witter, and W. Tolksdorf, Phys. Rev. B 27, 4375 (1983).

[23]P. Hansen, W. Tolksdorf, and K. Witter, IEEE Trans. Magn. 17, 3211 (1981).

[24]P. Hansen, M. Rosenkranz, and K. Witter, Phys. Rev. B 25, 4396 (1982).

[25]D. Mateika, in Current Topics in Materials Science, edited by E. Kaldis (North-Holland, New York, in press).

[26]W. Tolksdorf, G. Bartels, and H. J. Tolle, J. Cryst. Growth 52, 722 (1981).

[27]C. P. Klages and W. Tolksdorf, J. Cryst. Growth; C. P. Klages, W. Tolksdorf, and G. Kumpat, J. Cryst. Growth, in press.

[28]P. Willich, W. Tolksdorf, and D. Obertop, J. Cryst. Growth 53, 483 (1981).

[29]W. Tolksdorf, in Physics of Magnetic Garnets, edited by A. Paoletti (North-Holland, New York, 1978) p. 521.

[30]B. Strocka, P. Holst, and W. Toklsdorf, Philips J. Res. 33, 186 (1978).

[31]R. D. Shannon, Acta Crystallogr. A 32, 751 (1976).

[32]H. L. Glass and M. T. Elliott, J. Cryst. Growth 27, 253 (1974).

[33]S. Geller, H. J. Williams, G. P. Espinosa, R. C. Sherwood, and A. M. Gilleo, Appl. Phys. Lett. 3, 21 (1963).

[34]P. J. Page, private communication.

[35]T. J. A. Popma, A. M. van Diepen, and P. F. Bongers, J. Phys. Chem. Solids 35, 201 (1974).

[36]H. Takeuchi, Jpn. J. Appl. Phys. 13, 2059 (1974).

[37]H. Takeuchi, Jpn. J. Appl. Phys. 14, 1903 (1975).

[38]S. Geller and A. A. Colville, in Magnetism and Magnetic Materials—1974 (San Francisco), Proceedings of the 20th Annual Conference on Magnetism and Magnetic Materials, edited by C. D. Graham, G. H. Lander, and

J. J. Rhyne (AIP, New York, 1975), p. 372.

[39]P. J. Zanzucchi, in Heteroepitaxial Semiconductors for Electronic Devices, edited by G. W. Cullen and C. C. Wang (Springer, New York, 1978) p. 182.

[40]The crystals have been supplied by J. L. Page, Philips Research Laboratories, Redhill, England.

[41]A. B. Smith, Rev. Sci. Instrum. 39, 378 (1968).

[42]G. F. Dionne, J. Appl. Phys. 41, 2264 (1970).

[43]P. Hansen, J. Schuldt, and W. Tolksdorf, Phys. Rev. B 8, 4274 (1973).

[44]P. Hansen, J. Appl. Phys. 45, 3638 (1974).

[45]P. Hansen, in Physics of Magnetic Garnets, edited by A. Paoletti (North-Holland, New York, 1978), p. 56.

[46]S. Haussühl, D. Mateika, and W. Tolksdorf, Z. Naturforsch. 31a, 390 (1976).

[47]H. Miyajima, K. Sato, and T. Mizoguchi, J. Appl. Phys. 47, 4669 (1976).

[48]P. Hansen and K. Witter, Phys. Rev. B 27, 1498(1982).

[49]G. B. Scott, D. E. Lacklison, J. L. Page, and J. Hewett, Appl. Phys. 9, 71 (1976).

[50]G. F. Dionne, J. Appl. Phys. 47, 4220 (1976).

[51]P. Röschmann and P. Hansen, J. Appl. Phys. 52, 6257 (1981).

[52]S. Geller, in Physics of Magnetic Garnets, edited by A. Paoletti (North-Holland, New York, 1978), p. 1.

[53]W. P. Wolf, Phys. Rev. 108, 1152 (1957).

[54]H. Callen, J. Appl. Phys. 45, 2348 (1974).

[55]H. Callen, Mater. Res. Bull. 6, 931 (1971).

[56]E. M. Gyorgy, M. D. Sturge, and L. G. Van Uitert, in Magnetism and Magnetic Materials—1973 (Boston), Proceedings of the 19th Annual Conference on Magnetism and Magnetic Materials, edited by C. D. Graham and J. J. Rhyne (AIP, New York, 1974), p. 70.

[57]D. Linzen, S. Bormann, P. Görnert, R. Hergt, H. Pfeiffer, W. Schüppel, F. Voigt, and M. Wendt, Phys. Status Solidi A 43, 277 (1977).

[58]W. A. Crossley, R. W. Cooper, J. L. Page, and R. P van Stapele, Phys. Rev. 181, 896 (1969).